# Journal Pre-proof

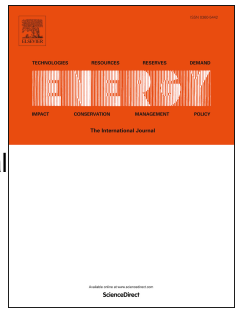

Modelling and optimization of a pilot-scale entrained-flow gasifier using artificial neural networks

Han Wang, Donovan Chaffart, Luis A. Ricardez-Sandoval

PII: S0360-5442(19)31771-2

DOI: https://doi.org/10.1016/j.energy.2019.116076

Reference: EGY 116076

To appear in: *Energy*

Received Date: 27 June 2019

Revised Date: 15 August 2019

Accepted Date: 5 September 2019

Please cite this article as: Wang H, Chaffart D, Ricardez-Sandoval LA, Modelling and optimization of a pilot-scale entrained-flow gasifier using artificial neural networks, *Energy* (2019), doi: https://doi.org/10.1016/j.energy.2019.116076.

# Modelling and Optimization of a Pilot-scale Entrained-Flow Gasifier using Artificial Neural Networks

Han Wang, Donovan Chaffart, Luis A. Ricardez-Sandoval[1]

*Department of Chemical Engineering, University of Waterloo, Waterloo, Canada, N2L 3G1*

## Abstract

This paper explores the construction and validation of an artificial neural network (ANN) in order to accurately and efficiently predict the performance of a pilot-scale gasifier unit. This ANN model consists of multiple sub-networks that individually predict each of the desired gasifier outputs as a function of key system parameters. The ANN was trained using data generated for a large set of randomly-generated input conditions from a pilot-scale gasifier reduced order model (ROM) developed previously. The fully-trained ANN was validated by comparing its performance to the aforementioned ROM model. The validated ANN model was subsequently implemented into two optimization studies in order to determine the operating conditions necessary to maximize the carbon conversion under different limitations for the peak temperature of the gasifier and to determine the ideal input conditions of maximizing both the carbon conversion and production of hydrogen gas which are two conflicting objectives. This case study further showcases the benefit of the ANN, which was able to obtain accurate predictions for the gasifier results similar to the results generated by the ROM model at a much lower computational cost.

**Keywords:** Artificial Neural Networks; Pulverized Coal Technology; IGCC Gasifier; Syngas Production; Multi-Objective Optimization

[1]Corresponding author. Tel.: + 1 519 888 4567x38667; fax.: + 1 519 888 4347. *E-mail Address:* laricard@uwaterloo.ca (L.A. Ricardez-Sandoval)

## 1. Introduction

Approximately one third of total $CO_2$ emissions at the present are produced from coal-fired electricity generation, making it the second largest production source of greenhouse gases.[1,2] The demand for coal-based power plants is expected to continue to rise over the next several decades, which is expected to increase $CO_2$ emissions and thus contribute negatively towards global warming. Motivated by the fight against climate change and the desire to reduce global greenhouse gas emissions, there is a current incentive and interest to develop and implement carbon capturing techniques and advanced pulverized coal combustion in the industry in order to reduce the footprint of coal energy production.[3,4] In advanced pulverized coal combustion, coal is finely-ground such that it will burn as easily and efficiently as natural gas. There are several different advanced pulverized-coal technologies already on the market, including the integrated gasification combined cycle (IGCC) power plant. The IGCC power generation system is an advanced power system consisting of a gasification and quench unit, a water-gas shift reactor, a purification unit, a gas turbine, a heat recovery steam generator, a steam turbine and an air separation unit. In the IGCC process, fuel, oxygen, and steam are fed into a gasification unit to produce raw syngas mainly consisting of CO, $H_2$ and $CO_2$. IGCC has a number of key benefits over other pulverized-coal technologies, such as higher fuel flexibility, higher efficiency, reduced production of solid wastes, lower $SO_x$, $NO_x$, and $CO_2$ emissions, marketable by-products, and higher energy output, which all have a positive benefit on air and water quality.[5]

One of the most important processes in an IGCC is the gasification unit, in which the solid coal is converted into syngas (i.e. CO and $H_2$). This syngas has a higher heating value than coal and thus it is a superior fuel to utilize in subsequent IGCC processes. As a result, there has been substantial interest in studying and optimizing the performance of IGCC gasification unit in

order to improve the efficiency of fuel and power generation, versatility, reliability, and economics in IGCC systems.[6,7,8] Computational fluid dynamics (CFD) models are often used to simulate gasifiers because of their ability to explicitly handle gasification flows and mixing and therefore provide sufficiently accurate predictions.[9] CFD modelling techniques have been frequently applied to simulate gasification and combustion in fluidized beds, and extensive reviews for this subject can be found in the literature.[9,10] Most notably, Fletcher et al. developed a CFD model to simulate the flow and reaction in an entrained flow gasifier that they built based on the CFX package, which is a useful tool for gasifier design and analysis.[11] Although CFD models are accurate and provide a more detailed outlook compared to other gasification simulation models, they are often found to be computational intensive which can significantly limit their implementation for optimization, online monitoring, and process control applications. This has motivated the development of alternative, computationally-efficient modelling techniques such as Reduced Order Models (ROMs),[12] equilibrium models,[13,14] and two-phase combustion models.[15] Sahraei et al. proposed a reactor network ROM which utilizes plug flow reactor (PFR) and continuous stirred tank reactor (CSTR) models to simulate the different zones inside an entrained-flow gasifier, which is the most common gasifier unit used in IGCCs.[12,16,17] Similarly, Shastri et al. proposed an approximate gasifier model developed in ASPEN Plus in order to perform optimization using the CAPE-OPEN stochastic simulation capability on the gasification unit of an IGCC system.[18] However, even though the ROMs and other equilibrium models require substantially lower computational costs compared to CFD models, they still require considerable numerical analysis and thus they are still computationally expensive for optimization, monitoring and online control applications.

Artificial neural network (ANNs) is an alternative modelling method that can be used to predict

the performance of the gasification unit in IGCCs at reduced computational costs. ANNs require short CPU times to predict the system outputs given a set of input parameters, and thus they are a computationally attractive tool for predicting and optimizing complex systems such as a gasifier when compared to the ROMs and CFD models.[16,19] As a result, there have been a handful of works within the literature that have applied ANNs to gasification systems.[20,21,22] Ongen et al. proposed an ANN model to observe variations in the syngas related to operational conditions in a tannery industry wastewater treatment sludge gasification system.[20] Mikulandric et al. analyzed the possibilities of neural networks to predict process parameters of a fixed bed gasifier in a biomass gasification process with high speed and accuracy.[21] Puig-Arnavat presented an ANN model for biomass gasification process in fluidized bed reactors.[22] Each of those works exemplifies how ANNs are a good and efficient mathematical tool for generating models to predict the input/output relationship between important parameters of gasification units. However, to the authors' knowledge, ANNs have not been previously used to build up a model and perform optimization on entrained flow gasifiers in IGCC system.

Motivated by this, the aim of this work is to produce an ANN model to describe and predict the behaviour between the main features of an IGCC pilot-scale gasification unit such as the composition, temperature distribution, and carbon conversion, and the main reactor inputs such as the inlet flowrates, inlet fuel temperature, and fuel composition. The proposed ANN model was trained and tested using sets of input and output data generated from a ROM model previously developed within our research group.[23,12,16,24] We optimized our ANN architecture by incrementing the number of neurons in each networks' hidden layers in order to obtain the ANN architecture with the minimum square error. Subsequently, we used the fully-developed

nonlinear ANN model to perform two different optimization studies on the gasifier system and gain insight on the optimal operation of this unit.

This paper is organized as follows. Section 2 describes the pilot-scale gasifier configuration which is modeled in this work and introduces the ROM used this study to model the gasification unit. Section 3 describes the ANN model implemented in this work and presents the optimization of the network architecture. In Section 4, the ANN model is validated through comparison to the ROM developed previously. Section 5 subsequently presents an optimization case studies of a pilot-scale gasifier under different peak temperature limitations using ANN-based optimization and compare the computational time to the ROM-based optimization. Section 6 describes a multi-objective optimization to maximize both the carbon conversion and the production of $H_2$ using the generated ANN model. Concluding remarks are provided at the end.

## 2. Pilot-Scale entrained-flow gasifier model

The entrained-flow IGCC gasifier system modeled in this work consists of a tonne-per-day (TPD) pilot-scale gasifier owned by CanmetENERGY, Natural Resources Canada, which is briefly illustrated in Fig.1.[25] This pilot gasifier is lined with refractory and insulation materials in order to reduce its heat loss, as it has a large surface area to volume ratio. As shown in Fig. 1, fuel, steam ($H_2O$), oxygen ($O_2$) and nitrogen ($N_2$) are fed into the gasifier to produce raw syngas. At the gasifier inlet, oxygen is injected through the burner by eight jets and mixed with the fuel stream at a high velocity. Subsequently, steam preheated to 500 K is passed through the outer burner annulus at a low velocity, and the fuel is carried through the reactor inlet by a stream of nitrogen carrier gas. The pet-coke's temperature often ranges from 270K to 330K before it is loaded into the gasifier, as the initial temperature significantly affects the gasifier temperature profile when the fuel is mixing with the steam. In addition, the composition of the pet-coke in the

fuel (i.e. the mass fraction of ash, volatiles, and moisture) plays a crucial role in the reaction process and the formation of the volatile products.

As mentioned above, IGCC gasifier models are conventionally modelled using CFD models[7,9,26], which can provide an accurate and detailed outlook for the gasification system but they can be extremely computationally expensive. This has motivated the development of more efficient modelling methods such as reduced order models (ROMs). These ROMs are an alternative approach that can be used to provide detailed information about the multi-phase flow structure of a gasification unit such as its solid particle concentration, composition, and temperature distribution along the length of the gasifier. Sahraei et al.[12,16] proposed a reactor network ROM consisting of different plug flow reactor (PFR) and continuous stirred tank reactor (CSTR) models to simulate each of the different zones at steady state inside the entrained-flow gasifier mentioned above. The key input parameters of the ROM are inlet flow rate of pet-coke, steam, oxygen and nitrogen, the initial temperature of the pet-coke, and the percent composition of ash, volatiles, and moisture within the pet-coke. The pet-coke composition contained a molar fraction of 0.046 ash, 0.127 volatiles, and 0.005 moisture and 0.822 carbon. The ROM was developed over an explicit input parameter range determined experimentally on the pilot-scale gasifier, and consequently the ROM is only valid for this specific range of operating conditions.

The performance of a gasifier can be described by the conversion of its reactants, the concentration of its desired products at the outlet, and the temperature distribution throughout the unit.[17] In the ROM model, the carbon conversion is the main important output parameter for characterizing the gasifier performance, as it serves to measure the fraction of solid coal converted into the more useful syngas form. In addition, the gasifier products, i.e. CO and $H_2$, provide a much lower heating value and require lower operating temperatures, and thus they are

able to achieve much greater efficiency than their solid fuel alternatives. Consequently, it is important to be able to predict the molar percentage of CO and $H_2$ in the outlet gas flow as a function of the input parameters. Another significant observable of the gasifier system is the internal temperature, which has a significant effect on the reactions taking place. Specifically, the peak temperature of the gasifier are monitored in order to keep it below the maximum temperature that the refractory brick layer within the gasifier can bear.[27] Furthermore, standard measurement devices such as thermocouples are often used in industrial reactors to monitor the temperature at key locations inside the unit. For the specific IGCC gasifier unit considered in the ROMs model work, there are four thermocouples located on the wall of the gasifier reactor, so that the operations can observe and monitor the temperature distribution at these discrete locations. The location of each thermocouple is detailed in Fig. 1.

The ROM reactor network considered in this work decomposes the gasifier system into three different types of zones referred to as the jet expansion zone (JEZ), external recirculation zone (ERZ), and down-stream zone (DSZ) regions, as outlined in the Fig. 2.

As shown in this figure, the JEZ and DSZ are modeled as plug flow reactors (PFRs) whereas the ERZ zones are modeled as continuous stirred tank reactors (CSTRs). Rather than solving the differential equations across the entire gasifier domain using CFD techniques, the ROM reduces the order of equations inside each gasifier zone, e.g. ERZ zones can be considered as a single node because of uniform particle and temperature distributions. In the JEZ region, the steam, and oxygen are suddenly expanded at the gasifier inlet, which causes the flow of fuel to spread out. When the flow reaches the gasifier wall, a portion of the stream recycles back to the top of the gasifier through the ERZ region while the rest of the stream flows towards the DSZ region at the bottom of the reactor. Inside each reaction zone, the gasifier's behaviour is simulated based on

the flow characteristics (i.e. whether they are mixed or laminar) and the one-dimensional governing equations of gas and solid phases for mass, energy, and momentum are solved for each zone to provide a distribution of different properties. The conservation equations of mass, energy and momentum used to simulate each zone of the gasifier are listed in Table 1 (see the Nomenclature section for the definition of the model parameters). As indicated in previous studies, the ROM used in this work was validated using both CFD simulation results and experimental data[12] obtained from CanmetENERGY's pilot-scale gasifier. A more detailed model description of the ROM as well as the descriptions for the model parameters presented in this table can be found elsewhere in the literature.[12,16] However, it is important to note that even though the ROMs require substantially lower computational costs compared to CFD models, they still require considerable numerical analysis and thus they are still computationally expensive for optimization, monitoring and online control applications.

## 3. ANN model development

In this work, an artificial neural network was developed to calculate the key outputs of the pilot-scale gasification unit such as the carbon conversion, outlet composition, peak temperature, and temperature at the thermocouples' location, as a function of the relevant system parameters, such as the inlet gas flowrates, the inlet temperature, and the fuel composition. The developed ANN consisted of a number of sub-ANNs that were each developed to predict the performance of each output parameter individually as a function of the inputs. The sub-ANNs were developed using a two-layer neural network structure that consisted of a single hidden layer with a tan-sigmoid transfer function and an output layer with a linear transfer function, as illustrated in Fig.3. Note that the two-layer neural network structure was selected as the basis for the ANN as it is considered to be the most suitable structure for nonlinear model fitting regression problems.[28]

Furthermore, no significant performance improvements were observed when the number of layers in the ANN sub-networks were increased. Each ANN was trained using data obtained from the ROM reported previously in Section 2.[12] The following sections will provide a brief overview of the ANN methodology implemented in this work. A general overview of the feedforward ANN structure and its backpropagation algorithm is provided, followed by a brief description of the gasifier variables that serve as the input and output parameters to the ANNs. Subsequently, the performance of various back-propagation algorithms on the ANN training are compared, and the optimal number of hidden layer neurons are determined for each ANN in order to optimize their predictive capabilities.

### 3.1 Feedforward Artificial Neural Network Overview

An ANN model consists of several layers of simple computing nodes, referred to as neurons, which predict different aspects of the input-output parameter relationship using nonlinear summing techniques. These layers typically consist of a number of hidden layers, as well as an output layer. The hidden layer of the ANN determines the relationship between the inputs and the outputs, and the values calculated by hidden layer neurons are subsequently fed to the next layer. In the output layer, a linear transfer function maps the hidden layer outputs onto the range of the desired output parameters. The neurons in each layer of the ANN are interconnected via a series of weighted connection lines, as illustrated in Fig. 3. Each neuron consists of a weighted linear function and a transfer function, as denoted in Fig. 4. Note that in this figure, $\xi_i$ denotes the linear weights function for the $i^{th}$ neuron, which is defined as the sum of each of the $j^{th}$ outputs from the previous layer (input layer); whereas $x_j$ denote the input value of the $j^{th}$ input parameter from the $j^{th}$ neuron in the input layer, and the terms $w_{i,j}$ and $b_i$ in $\xi_i$ denote the weight and bias values applied to the $i^{th}$ neuron, respectively. Furthermore, the function $f$ denotes the transfer

function applied to $\xi_i$. The transfer function applied in the hidden layers of an ANN usually consists of a sigmoidal function that maps $\xi_i$ onto a nonlinear curve, whereas a linear transfer function is typically applied to the output layer to map $\xi_i$ onto the range of the output parameters. In order for the ANN to function properly, it is necessary to adjust the weights and the biases of each neuron so that the ANN can predict the output results for a given set of input parameters.[29,30] This can be accomplished through supervised training, in which the network is provided with a series of input parameters and their corresponding output values. At the beginning of the network training, each of the weights and biases ($w_{i,j}$ and $b_i$) are randomly generated from a uniform distribution within the active range of the tangent sigmoid transfer function and their values are subsequently updated via backpropagation (BP).[31,32]

ANNs are a machine-learning approach that seeks to determine the relationship between the input and output parameters. An adequately-trained neural network will have no access to the original training data after training has been completed and therefore it must rely on the trained neuron functions in order to predict a system's outputs. Consequently, it is imperative to train an ANN such that it does not simply memorize the training data but rather so it learns to predict the relational patterns between the input and output parameters. In order to avoid overfitting in the neural network model, it is necessary to analyze the ANN performance during training in order to prevent the network from simply memorizing the training data. For the ANN training algorithm implemented in this work, an early stopping method is utilized that sub-divides the provided input-output dataset into three parts: the training set, the validation set, and the testing set.[33,34] The training set is used for network training, which optimizes the weights and biases of each neuron so as to minimize the error between the ANN model outputs and the training data outputs. The validation and testing set are used to validate the performance of the ANN model.

Specifically, the network is tested using the validation set during training in order to evaluate its generalization. On the other hand, the network is only validated using the testing data after training has been completed in order to validate its prediction capabilities for conditions that the network has not seen previously. Note that the validation and testing sets ensure that the network is able to sufficiently predict the relationship between the input and output parameters for operating conditions outside of the training dataset. As a result, they serve as an important diagnostic of the network's generalization and its ability to predict outputs for conditions outside of the training dataset. Consequently, these sets can be used to stop the network training before the training data is merely memorized and thus they provide a measure of guarantee that the fully-trained ANN model is not merely interpolating between the training data. Further details about the early stopping method are reported elsewhere in the literature.[35]

### 3.2 Input and output training data

The carbon conversion ($T_1$), the molar composition of CO ($T_2$) and $H_2$ ($T_3$), peak temperature of the gasifier ($T_4$), and the temperature at the four thermocouples located on the wall of the gasifier reactor (i.e. $T_5$-$T_8$), all serve as the desired measurable outputs for the gasifier system, and thus are considered as the key output parameters (**T**) to be predicted using the ANN model. On the other hand, the key input parameters (**P**) that affect the gasifier performance are the injected fuel flowrate ($P_1$), the oxygen flowrate ($P_2$), the nitrogen flowrate ($P_3$), the steam flowrate ($P_4$), the initial fuel temperature ($P_5$), and the fuel compositions of ash ($P_6$), volatiles ($P_7$), and moisture ($P_8$). Consequently, these parameters serve as the inputs which the ANN model would use to predict the desired outputs. More information about each of these input and output parameters can be found in Section 2. Furthermore, Table 2 provides a comprehensive list of the input (**P**) and output (**T**) parameters, their nominal values, and the corresponding minimum and maximum

input parameter values over which the ANN was trained. These input ranges were determined experimentally using the ROM in order to guarantee that they are feasible and capable of obtaining reasonable results for both the ROM and ANN models.[12,23] Note that the parameter ranges reported in this table only showcase the values over which the developed ANN model can be applied, and therefore the gasifier behaviour was not analyzed under these conditions. Additionally, note that the fuel composition parameters ($P_6$, $P_7$, & $P_8$) cannot be accurately controlled, as the fuel composition can only be coarsely altered by changing the type of coal used. Consequently, the ranges for these parameters were determined by applying a $\pm 5\%$ fluctuation around the expected values for each fuel component, as this was determined to provide satisfactory composition bounds via laboratory experiments.[16]

In order to train the ANN model, it is necessary to generate a large number of data points for each model output using various combinations of each of the input parameters. For the study presented in this work, the ANN data was generated using 8,000 combinations of input parameters randomly generated from a uniform distribution, between their upper and lower bounds as listed in Table 2. Trial-and-error simulations were performed to determine a suitable data set for the identification of the ANNs. Increasing the sample size beyond 8,000 samples increases the computational effort but it does not improve the prediction capabilities of the ANNs. Each of these input parameter combinations were passed through the ROM in order to determine their corresponding output parameter values; these input and output parameters were subsequently paired up and fed into the training process used to generate the ANNs model.

### 3.3 Selection of back-propagation algorithm

The backpropagation method is one of the most crucial concepts for enabling the self-learning capabilities of an ANN.[36] This methodology refers to the ability of a neural network to adjust the

values of its weights and biases based on the error in the network outputs.[37] As a result, it is important to select a good back-propagation method to ensure that the network can accurately and efficiently learn to predict the outputs of a system given a set of inputs without being subject to overfitting.

In this study, we compared eight different BP algorithms with the aim of choosing the best fitting algorithm for the gasifier data collected. Each BP algorithm considered is not discussed within this paper for the sake of brevity; further discussion about these algorithms can be found within the literature.[38,39] Each BP algorithm was used to train a two-layer ANN with 10 neurons in the hidden layer in order to predict the outlet CO composition ($T_2$) as a function of each of the input parameters **P**.

The results of the network training for each BP algorithm are presented in Table 3. These results reveal that the Levenberg-Marquardt algorithm is the best BP algorithm for the ANN system considered in this work, as it managed to achieve the lowest mean squared training error with a minimum value of $2.30\times10^{-7}$. Furthermore, the training was stopped after 138 epochs. Even though the Scaled conjugate gradient and One-step secant BP can achieve the similar error magnitude and R value to the Levenberg-Marquardt algorithm, both of them needed more training iterations which means that they required more time to obtain the optimal weights and bias of their corresponding ANN models. The weakest BP training algorithms are Gradient descent with momentum and Gradient descent, which needed the most iteration numbers to find the optimal weights and bias and produced the largest magnitude of mean squared errors of the trained ANN models. These results are further validated in Fig. 5 which showcases the training and validation mean square errors at each epoch of the network training using the Levenberg-Marquardt algorithm. This figure additionally illustrates that the network training results were

reasonable, as the train and validation errors both displayed similar characteristics, and these two errors did not change significantly upon further training. As shown in Fig. 5, the validation error reached the minimum best validation mean squared error (MSE), when MSE of validation does not decrease for six consecutive epochs. As a result, the Levenberg-Marquardt algorithm was implemented to train the ANN model developed in this work.

### 3.4 Neural network structure

The aim of this section is to perform optimization on the number of hidden layer neurons for each of the eight sub-ANNs developed in this work to predict each gasifier output. Each sub-network was developed using the two-layer architecture described previously, using the Levenberg-Marquardt algorithm for back-propagation. In this study, each sub-network was initialized with a hidden layer containing only a single neuron, and the sub-networks were trained to predict each of the model outputs as a function of the inputs. Subsequently, the number of neurons in each hidden layer was incremented by one and the networks were re-trained using the same data. This data was used to calculate the mean squared validation and testing errors for each network as a function of the number of hidden layer neurons. This process was repeated until the sub-network was observed to be memorizing the data, (i.e. when sub-network's validation error decreased but its testing error was observed to increase), at which point the optimization process was terminated for that network.

The results of the identification of the optimal structure for each of the ANNs developed in this work are shown in Table 4. The mean squared errors of carbon conversion ($T_1$), CO composition ($T_2$) and $H_2$ composition ($T_3$) are less than $1\times10^{-6}$, which is sufficiently small, while mean squared errors of peak temperature ($T_4$) and thermocouple temperatures ($T_5$-$T_8$) are notably larger than the remaining output parameter errors due to the higher orders of magnitude of values

compared to composition and conversion and these errors are still less than $1\times10^2$. Furthermore, the maximum percentage errors between the actual output by trained ANN and the target output generated by ROM for test set and validation set in training process are sufficiently low, i.e. < 3% for all the output parameters except for the temperature at thermocouple 1 ($T_5$). Even though the maximum percentage error of temperature at thermocouple 1 ($T_5$) are 6.0075% and 5.2366% for test set and validation set separately, which are larger than the errors of other output parameters, they are still relatively low enough and acceptable. Note that the maximum percentage errors between test and validation set are similar to each other for each output parameter, which means that there's no overfitting in each ANN model. Figure 6 illustrates the optimal neural network structure for each of the sub-networks and provides the general framework of the ANN model considered in this study. Furthermore, Fig. 7 showcases the linear regression analysis between the ANN outputs generated using the optimal number of hidden neurons and the corresponding output targets for $T_2$, the molar fraction of CO at the outlet. As can be seen by these results, the ANN can adequately predict the target output data given the non-linear relationship between the inputs and outputs for the output parameter ($T_2$). A similar performance was observed for the rest of the output parameters but it is not shown here for brevity. A complete list of the weights and biases for each sub-ANN can be found in the supplementary material. These weights highlight that the gasifier conversion and temperature profile are strongly affected by the oxygen flowrate, mildly affected by the inlet fuel temperature, and inversely affected by the fuel flowrate. In addition, the peak temperature is inversely affected by the steam flowrate. Similarly, the outlet CO composition is strongly affected by the oxygen and steam flowrate and inversely affected by the fuel flow rate and the percent volatile composition within the fuel, whereas the outlet $H_2$

composition experiences the opposite trends. These are in similar agreement with the trends reported elsewhere within the literature[40].

## 4. Model Validation

The objective of this section is to test and validate the performance of the ANN model described previously in Section 2. The ANN's performance was evaluated with respect to the ROM which has been reported previously in the literature.[12,16] Note that this ROM has further been previously validated through comparison against CFD and experimental results, as detailed in the aforementioned articles. Note that the accuracy of the ANN is dependent on the predictive capabilities achieved via the training process described in Section 2. Therefore, the ANN output performance was validated subject to changes in each of the input parameters **P** listed in Table 2. In order to ensure good generalization for each ANN model, the trained ANN model was tested using 2,500 combinations of input parameter values that had not been previously used during the network training. As a result, each combination of the eight input parameters utilized in this study was generated afresh via random selection from a uniform distribution within the parameter ranges showcased in Table 2, i.e. the parameter ranges over which the networks were trained. Each of these combinations were inspected *a priori* in order to ensure that they were different from the data used to train the ANN model and its sub-networks. Table 5 presents 10 out of the 2,500 combinations of input parameters used to validate the performance of the ANN. The performance of both the ROM and ANN models for these ten combinations of input parameters, as assessed through each of the eight output parameters, are illustrated in Fig. 8. Note that the outputs for the remaining 2,490 sample points used for model validation are not shown here for the sake of brevity; however, their results were comparable to those illustrated in

Fig. 8. In addition, Table 6 displays the sum of squared errors of the outputs between the results of the ROM and the ANN model for the full batch of 2,500 input operating condition combinations. These results show that the ANNs model is able to adequately capture the behavior of the gasifier unit, and that the ANN model is not overfitting. As shown in Fig. 8, the profile of each eight outputs determined using the ROM match those determined using each of the ANN sub-networks. Furthermore, Table 6 shows that the errors in the ANN-predicted outputs remain sufficiently low, i.e. $< 2.5 \times 10^{-3}$ and $< 6 \times 10^{-2}$ for the mean and maximum relative errors respectively for all eight output parameters. Note that the sum of squared errors for each of the temperatures (i.e. the peak temperature and the temperatures at the thermocouple locations), as shown in Table 6, are notably larger than the remaining output parameter errors; this is because the temperatures are of higher orders of magnitude compared to the other outputs, and thus they are subject to larger absolute errors. With regards to the computational cost, the ROM model and the ANN model required on average about 257s and $1.6 \times 10^{-3}$s of CPU time per simulation, respectively (Intel® Core™ i7-4770 CPU @ 3.40Hz, 3392 Mhz, 4 Core(s), 8 Logical Processor(s)). This difference in the computational time illustrates that the ANN is approximately $1.6 \times 10^{5}$ times faster than the ROM model. This demonstrates that the ANN is significantly more computationally efficient compared to the ROM, while achieving sufficiently similar results. Overall, this validation study demonstrates that the ANN model is able to predict the steady state behavior of the gasification reactor accurately and can be used to perform optimization studies.

## 5. Optimization: Carbon Conversion

Integrated Gasification Combined Cycle (IGCC) system using coal gasification is an crucial component of future energy alternatives. Since gasification is the most important component of

this system, it is particularly critical to understanding the operation and optimizing the gasification unit.[41] In industrial applications, the performance of a gasification unit in an IGCC plant is characterized by its conversion of carbon ($T_1$) into gaseous products such as CO, $CO_2$ and $CH_4$; as a result, it is crucial to manufacture IGCCs that meet or exceed specific carbon conversion requirements in order to maximize the gasifier performance.[42,43] Note that the peak temperature of the gasifier reactor should be constrained to be within a reasonable range to avoid damaging the refractory wall due to the high temperature. For different gasifier reactor types, the material of the reactor wall would be different and therefore, the constraints of the peak temperature of gasifier can be adjusted so that they do not impose a safety hazard. Motivated by this, the first objective of this section is to optimize the gasifier carbon conversion at the reactor outlet under different peak temperature limitations using the ANN gasification model developed in Section 3. This optimization study was performed with respect to each of the input parameters **P** mentioned in Section 3.2 according to the following optimization formulation:

$$\max_{\mathbf{P}} T_1(\mathbf{P}) \quad (1)$$

Subject to:
$ANN\ model$

$$T_4(\mathbf{P}) \leq T_{4,max}$$

$$\mathbf{P}_{min} \leq \mathbf{P} \leq \mathbf{P}_{max}$$

where $\mathbf{P}_{min}$ and $\mathbf{P}_{max}$ represents the lower and the upper bounds for all the eight input parameters considered in $\mathbf{P}$, which can be found in Table 2. $T_{4,max}$ denotes the maximum allowable temperature that the refractory wall can bear, and the function of carbon conversion ($T_1$) is a nonlinear function estimated by the ANN gasification model. The above optimization formulation was performed using different bounds of the peak temperature, i.e. $T_{4,max}$ was set to

2,400K, 2,500K, 2,600K, and 2,700K. This was done to obtain an insight to the effect of peak temperature limitation on the optimized results of carbon conversion and the remaining gasifier parameters. The results of the input parameters obtained from the different optimization runs were additionally fed into the ROM in order to validate the results of the ANN model, and the corresponding results of carbon conversion from ROM are similar to the optimized carbon conversion values run by ANN model. Then, these results from optimization by ANN were compared to the nominal reactor conversion predicted by the ROM using the nominal input values presented in Table 2. Note that the results from this optimization study were compared to the training data in order to ensure that they were not included among the original data used to train and validate the network.

The results of the optimization study are presented in Table 7. As can be seen by these results, the maximum carbon conversion increases correspondingly with the limitations of peak temperature rising. Notably, the maximum carbon conversion increases drastically from 0.8111 to 0.9702 when the limitation of peak temperature changes from 2,400K to 2,600K. While peak temperature limitation increases from 2,600K to 2,700K, the maximum carbon conversion does not increase notably (differences noted beyond five decimal digits). This result is consistent with the results obtained by ROM, as the percent error in the optimal carbon conversion between both modelling methods remain below 0.3% for the four different peak temperature limitation case studies considered here. At the nominal operating conditions ($\mathbf{P}_{nom}$) listed in Table 7, the ROM predicted a carbon conversion of 0.9134, which is about 5.85% lower than the value obtained from the present optimization case study (Case 3 & Case 4 in Table 7). Note that according to the results in Table 7, higher carbon conversions are associated with higher steam flow rates; thus, increasing the steam flow rates can promote higher carbon conversions. The results from

the optimization also indicate that, as the maximum allowed peak temperature constraint is relaxed, the carbon conversion tends to increase significantly up until it reaches approximately 0.97 conversion, which seems to be the highest conversion that can be achieved for the nominal operation of the pilot-scale gasification unit considered in this study, when the limitation increase beyond $T_{4,max}$ = 2,600K, the conversion does not tend to change significantly. Furthermore, the results also illustrate that a lower fuel flowrate, a higher steam flowrate, a higher inlet fuel temperature, and higher mass fraction of ash, volatiles and moisture would also lead to a higher carbon conversion. As a result, the optimization study predicts that higher ratios of steam and oxygen to pet-coke are required in order to obtain higher carbon conversions. Table 7 additionally shows that the optimization results obtained using the ANNs are similar to the values obtained using the ROM, which demonstrates that the ANN is able to accurately predict the gasifier outputs for optimization applications. Each of the optimization runs required an averaged CPU time of 0.0808s, however, the same optimization study using the ROM required 7,573s; i.e. at least four orders of magnitude the time needed to perform the same optimization using the ANN.

## 6. Multi-objective optimization

Another key performance indicator of an IGCC gasifier is the composition of the syngas it produces. Specifically, specific syngas components such as $H_2$ require lower operating conditions than others, and it is thus beneficial to maximize the molar fraction of hydrogen in the final syngas composition so as to improve its efficiency. In an ideal gasifier system, it is desirable to maximize both the carbon conversion and the production of $H_2$. However, these two objectives have been observed to be in conflict with each other, as the input conditions required to maximize carbon conversion negatively impact the hydrogen production, and vice versa.[12]

Motivated by this, a second optimization study was performed with the aim to analyze the relationship and determine the optimal trade-off conditions between these two conflicting objectives. This multi-objective optimization study was performed with respect to each of the input parameters **P** mentioned in Section 3.2 according to the following optimization formulation:

$$\max_{\mathbf{P}}[(1-w)\,T_1(\mathbf{P}) + wT_3(\mathbf{P})] \quad (2)$$

Subject to:
$ANN\ model$

$T_4\,(\mathbf{P}) \leq T_{4,max}$

$\mathbf{P}_{min} \leq\ \mathbf{P} \leq \mathbf{P}_{max}$

where the parameter $w$ is a weight which denotes the significance of each of the individual objective functions, i.e. carbon conversion ($T_1$) and hydrogen molar fraction in outlet ($T_3$). In the above optimization formulation, the maximum allowed peak temperature was fixed at $T_{4,max} =$ 2,600K based on the optimization results obtained for the first case study discussed above. Furthermore, the upper and lower bounds $\mathbf{P_{max}}$ and $\mathbf{P_{min}}$ are defined by the values listed in Table 2. For this multi-objective optimization study, the weight parameter $w$ was changed from 0 to 1 by increments of 0.1. The results of the multi-objective optimization obtained using the ANN model were validated by running the ROM as shown in Table 8. Note that the errors between the two modeling methods remained below 2.2%, showcasing that the ANN is capable of predicting the gasifier behaviour with sufficient accuracy compared to the ROM. Fig. 9 provides a graphical illustration of the pareto front for the feasible search space accessible to the gasifier model that is formed based on the solutions to problem (2). As indicated in this figure and in Table 8, when $w$ increases, the mole fraction of $H_2$ in the outlet syngas increases whereas the carbon conversion decreases, as was expected. Note that since the carbon conversion values ($T_1$) are much larger

than the hydrogen molar fraction values ($T_3$), there is a slowly-decreasing trend of the results of carbon conversion between $w$ = 0 and $w$ = 0.8. When $w$ reaches 0.9, the value of $wT_3(\mathbf{P})$ is similar to $(1-w)T_1(\mathbf{P})$, and consequently the optimized $H_2$ fraction begins to rise significantly whereas the carbon conversion starts to decrease drastically corresponding to the notable decrease in the oxygen-to-fuel ratio at $w$ = 0.9.

In order to determine the ideal trade-off point between the carbon conversion and the hydrogen production, the ANN gasifier model was implemented into a 1-norm bi-objective optimization scheme. This optimization approach seeks to minimize the 1-norm distance between the feasible search space, as defined by the pareto front, and the utopia point (i.e. the infeasible point that optimally satisfies both objectives simultaneously),[44] in order to determine which set of feasible conditions yield results that are closest to the utopia point (measured in terms of a 1-norm distance). The 1-norm minimization problem can be formulated as follows:

$$\min_{\mathbf{P}} \left[ \frac{T_{1,max} - T_1(\mathbf{P})}{T_{1,max} - T_{1,min}} + \frac{T_{3,max} - T_3(\mathbf{P})}{T_{3,max} - T_{3,min}} \right] \quad (3)$$

Subject to:

$ANN\ model$

$T_4(\mathbf{P}) \leq T_{4,max}$

$\mathbf{P}_{min} \leq \mathbf{P} \leq \mathbf{P}_{max}$

where $T_{1,max}$ and $T_{3,max}$ denote the maximum conversion and $H_2$ molar fractions obtainable within the optimization constraints of problem (2) and define the utopia point, $(T_{1,max}, T_{3,max})$. Note that the maximum conversion ($T_{1,max}$) and minimum $H_2$ molar fraction ($T_{3,min}$) values are obtained by solving a single-objective optimization study that maximizes the carbon conversion, i.e. when $w = 0$ in problem (2); similarly, the minimum conversion ($T_{1,min}$) and maximum $H_2$

fraction ($T_{3,max}$) values are obtained by solving the optimization study that maximizes the hydrogen production, i.e. when $w = 1$. In addition, the constraint parameters $\mathbf{P}_{min}$, $\mathbf{P}_{max}$, and $T_{4,max}$ were fixed to the same values used in problem (2). The results of this optimization study are listed in Table 8 (1-norm); in addition, the utopia point and the optimal trade-off point are denoted in Fig. 9. Under these optimal conditions, the carbon conversion $T_1 = 0.7494$ is at 52.2% of the utopia point conversion, whereas the molar fraction of $H_2$ in the outlet syngas $T_3 = 0.265$ is at 42.7% of the syngas hydrogen fraction at the utopia point, as shown in the Fig. 9. These results reveal that it is not possible to significantly improve the hydrogen production within the gasifier without also noticeably reducing the carbon conversion. Note that the ANN model only required about 0.1617s of CPU time to determine the optimized results for the multi-objective optimization described above. However, it is challenging to conduct the same optimization study using the ROM model due to the computation costs; hence, this demonstrates that the ANN is significantly more computationally efficient compared to the ROM, while achieving sufficiently similar results. Hence, the optimization using ANN shows that it is particularly efficient and accurate to perform optimization studies on the pilot-scale gasification unit.

## 6. Conclusions

The main objective of this work was to build an ANN consisting of eight sub-networks in order to predict the key outputs of an IGCC gasification system as a function of eight key system parameters. These sub-ANNs were constructed using a two-layer structure consisting of a single hidden layer in addition to the output layer. The number of neurons in the hidden layer were determined via optimization for each network. In addition, tests were performed to determine which back-propagation algorithm would provide the fastest and most reliable network training. The networks were each trained by a series of input/output data generated using a ROM

developed in a previous study. The ANN was successfully validated and was able to accurately predict the gasifier outputs at significantly lower computational costs compared to the ROM model. The ANN was subsequently used to perform two different optimization studies on the pilot-scale gasifier unit. In the optimization studies, we found that increasing the peak temperature limitation of the reactor can lead to a higher maximum carbon conversion, and from the utopia point of the multi-objective optimization, it seems unlikely to improve $H_2$ production significantly without reducing the carbon conversion within the gasifier. The results also show that the computational time of the optimization by ANN is at least four orders of magnitude faster when compared to the ROM-based optimization. Accordingly, as part of the future work, we can extend the application of ANNs to model the transient behaviour of a gasification system and perform online optimization and control of this system.

## Acknowledgements

The authors of this paper would like to graciously acknowledge the Natural Sciences and Engineering Research Council of Canada (NSERC) for their support granted for this research.

## References


(1) Williams, G. A.; Aaberg, T. M. Techniques of Scleral Buckling. *Retin. Fourth Ed.* **2005**, *3–3*, 2035–2070. https://doi.org/10.1016/B978-0-323-02598-0.50124-5.

(2) Betancourt-Torcat, A.; Elkamel, A.; Ricardez-Sandoval, L. A Modeling Study of the Effect of Carbon Dioxide Mitigation Strategies, Natural Gas Prices and Steam Consumption on the Canadian Oil Sands Operations. *Energy* **2012**, *45* (1), 1018–1033. https://doi.org/10.1016/j.energy.2012.06.043.

(3) Yeh, S.; Rubin, E. S. A Centurial History of Technological Change and Learning Curves for Pulverized Coal-Fired Utility Boilers. *Energy* **2007**, *32* (10), 1996–2005. https://doi.org/10.1016/j.energy.2007.03.004.

(4) Buchan, B.; Cao, C. *Coal-Fired Generation: Proven and Developing Technologies*; 2004.

(5) National Energy Technology Laboratory. *Life Cycle Analysis: Integrated Gasification Combined Cycle (IGCC) Power Plant*; 2010. https://doi.org/DOE/NETL-403-110209.

(6) Christou, C.; Hadjipaschalis, I.; Poullikkas, A. Assessment of Integrated Gasification Combined Cycle Technology Competitiveness. *Renew. Sustain. Energy Rev.* **2008**, *12* (9), 2452–2464. https://doi.org/10.1016/j.rser.2007.06.010.

(7) Luyben, W. L.; Robinson, P. J. A Simple Gasifier Model That Runs in Aspen Dynamics. *AIChE Annu. Meet. Conf. Proc.* **2008**, 7784–7792.

(8) Biagini, E.; Bardi, A.; Pannocchia, G.; Tognotti, L. Development of an Entrained Flow Gasifier Model for Process Optimization Study. *Ind. Eng. Chem. Res.* **2009**, *48* (19), 9028–9033. https://doi.org/10.1021/ie801804g.

(9) Chui, E. H.; Majeski, A. J.; Lu, D. Y.; Hughes, R.; Gao, H.; McCalden, D. J.; Anthony, E. J. Simulation of Entrained Flow Coal Gasification. *Energy Procedia* **2009**, *1* (1), 503–509. https://doi.org/10.1016/j.egypro.2009.01.067.

(10) Singh, R. I.; Brink, A.; Hupa, M. CFD Modeling to Study Fluidized Bed Combustion and Gasification. *Appl. Therm. Eng.* **2013**, *52* (2), 585–614. https://doi.org/10.1016/j.applthermaleng.2012.12.017.

(11) Fletcher, D. F.; Joseph, S. D. A CFD Based Combustion Model of an Entrained Flow Biomass Gasifier. **2006**, *24* (2000), 165–182.

(12) Sahraei, M. H.; Duchesne, M. A.; Yandon, R.; Majeski, A.; Hughes, R. W.; Ricardez-sandoval, L. A. Reduced Order Modeling of a Short-Residence Time Gasifier. **2015**, *161*, 222–232. https://doi.org/10.1016/j.fuel.2015.07.096.

(13) Aggarwal, M.; Balaji, S.; Ydstie, B. E. Invariant Based Modeling and Control of Multi-Phase Reactor Systems. *J. Process Control* **2011**, *21* (10), 1390–1406. https://doi.org/10.1016/j.jprocont.2011.07.008.

(14) Mahishi, M. R.; Goswami, D. Y. Thermodynamic Optimization of Biomass Gasifier for Hydrogen Production. *Int. J. Hydrogen Energy* **2007**, *32* (16), 3831–3840. https://doi.org/10.1016/j.ijhydene.2007.05.018.

(15) Kaushal, P.; Pröll, T.; Hofbauer, H. Model for Biomass Char Combustion in the Riser of a Dual Fluidized Bed Gasification Unit: Part II Model Validation and Parameter Variation. *Fuel Process. Technol.* **2008**, *89* (7), 660–666. https://doi.org/10.1016/j.fuproc.2007.12.009.

(16) Sahraei, M. H.; Duchesne, M. A.; Boisvert, P. G.; Hughes, R. W.; Ricardez-Sandoval, L. A. Reduced-Order Modeling of a Commercial-Scale Gasifier Using a Multielement Injector Feed System. *Ind. Eng. Chem. Res.* **2017**, *56* (25), 7285–7300.

https://doi.org/10.1021/acs.iecr.7b00693.
(17) Sahraei, M. H.; Mccalden, D.; Hughes, R.; Ricardez-sandoval, L. A. A Survey on Current Advanced IGCC Power Plant Technologies , Sensors and Control Systems. *FUEL* **2014**, *137*, 245–259. https://doi.org/10.1016/j.fuel.2014.07.086.
(18) Shastri, Y.; Diwekar, U. Stochastic Modeling for Uncertainty Analysis and Multiobjective Optimization of IGCC System with Single-Stage Coal Gasification. *Ind. Eng. Chem. Res.* **2011**, *50* (9), 4879–4892. https://doi.org/10.1021/ie101355x.
(19) Arcotumapathy, V.; Alenazey, F.; Adesina, A. A. Artificial Neural Network Modeling of Forced Cycling Operation between Propane Steam Reforming and CO2 Carbon Gasifier. *Catal. Today* **2011**, *164* (1), 275–281. https://doi.org/10.1016/j.cattod.2010.12.027.
(20) Ongen, A.; Kurtulus Ozcan, H.; Arayici, S. An Evaluation of Tannery Industry Wastewater Treatment Sludge Gasification by Artificial Neural Network Modeling. *J. Hazard. Mater.* **2013**, *263*, 361–366. https://doi.org/10.1016/j.jhazmat.2013.03.043.
(21) Mikulandrić, R.; Lončar, D.; Böhning, D.; Böhme, R.; Beckmann, M. Artificial Neural Network Modelling Approach for a Biomass Gasification Process in Fixed Bed Gasifiers. *Energy Convers. Manag.* **2014**, *87*, 1210–1223. https://doi.org/10.1016/j.enconman.2014.03.036.
(22) Puig-Arnavat, M.; Hernández, J. A.; Bruno, J. C.; Coronas, A. Artificial Neural Network Models for Biomass Gasification in Fluidized Bed Gasifiers. *Biomass and Bioenergy* **2013**, *49*, 279–289. https://doi.org/10.1016/j.biombioe.2012.12.012.
(23) Sahraei, M. H.; Yandon, R.; Duchesne, M. A.; Hughes, R. W.; Ricardez-Sandoval, L. A. Parametric Analysis Using a Reactor Network Model for Petroleum Coke Gasification. *Energy and Fuels* **2015**, *29* (11), 7681–7688. https://doi.org/10.1021/acs.energyfuels.5b01731.
(24) Sahraei, M. H.; Duchesne, M. A.; Hughes, R. W.; Ricardez-Sandoval, L. A. Experimental Assessment, Model Validation, and Uncertainty Quantification of a Pilot-Scale Gasifier. *Ind. Eng. Chem. Res.* **2016**, *55* (25), 6961–6970. https://doi.org/10.1021/acs.iecr.6b00692.
(25) CanmetENERGY research service. <http://www.nrcan.gc.ca/sites/www.nrcan.gc.ca/files/canmetenergy/files/pubs/Gasification_eng.pdf> [Cited 12.01.15].
(26) Chui, E. H.; Majeski, A. J.; Lu, D. Y.; Hughes, R.; Gao, H.; McCalden, D. J.; Anthony, E. J. Simulation of Entrained Flow Coal Gasification. *Energy Procedia* **2009**, *1* (1), 503–509. https://doi.org/10.1016/j.egypro.2009.01.067.
(27) Pedersen, L. S.; Breithaupt, P.; Dam-Johansen, K.; Weber, R. Residence Time Distributions in Confined Swirling Flames. *Combust. Sci. Technol.* **1997**, *127* (1–6), 251–273. https://doi.org/10.1080/00102209708935696.
(28) Ning Wang; Meng Joo Er; Min Han. Generalized Single-Hidden Layer Feedforward Networks for Regression Problems. *IEEE Trans. Neural Networks Learn. Syst.* **2014**, *26* (6), 1161–1176. https://doi.org/10.1109/tnnls.2014.2334366.
(29) Dayhoff, J. E.; Deleo, J. M. Opening the Black Box. **2001**, 1615–1635.
(30) Davidian, D. Feed-Forward Neural Network. **1995**, US5438646 A.
(31) Amardeep, R. Training Feed Forward Neural Network With Backpropogation Algorithm. *Int. J. Eng. Comput. Sci.* **2017**, *6* (1), 19860–19866. https://doi.org/10.18535/ijecs/v6i1.03.
(32) Yu, X.; Efe, M. O.; Kaynak, O. A General Backpropagation Algorithm for Feedforward Neural Networks Learning. *IEEE Trans. Neural Networks* **2002**, *13* (1), 251–254. https://doi.org/10.1109/72.977323.
(33) Chaffart, D.; Ricardez-Sandoval, L. A. Optimization and Control of a Thin Film Growth

Process: A Hybrid First Principles/Artificial Neural Network Based Multiscale Modelling Approach. *Comput. Chem. Eng.* **2018**, *119*, 465–479. https://doi.org/10.1016/j.compchemeng.2018.08.029.

(34) Benardos, P. G.; Vosniakos, G. C. Optimizing Feedforward Artificial Neural Network Architecture. *Eng. Appl. Artif. Intell.* **2007**, *20* (3), 365–382. https://doi.org/10.1016/j.engappai.2006.06.005.

(35) Bashir, Z. A.; El-Hawary, M. E. Applying Wavelets to Short-Term Load Forecasting Using PSO-Based Neural Networks. *IEEE Trans. Power Syst.* **2009**, *24* (1), 20–27. https://doi.org/10.1109/TPWRS.2008.2008606.

(36) Wechsler, H. *Computation, Learning, and Architectures*; 1992; Vol. 2.

(37) Kuldip Vora, S. Y. A Survey on Backpropagation Algorithms for Feedforward Neural Networks. *Int. J. Eng. Vor. S. Y. (2014). A Surv. Backpropagation Algorithms Feed. Neural Networks. Int. J. Eng. Dev. Res. (IJEDR), 1(3), 193–197. Dev. Res.* **2014**, *1* (3), 193–197.

(38) Maier, H. R.; Dandy, G. C. Understanding the Behaviour and Optimising the Performance of Back-Propagation Neural Networks : An Empirical Study. **1998**, *13*, 179–191.

(39) Ozkaya, B.; Demir, A.; Bilgili, M. S. Neural Network Prediction Model for the Methane Fraction in Biogas from Field-Scale Landfill Bioreactors. *Environ. Model. Softw.* **2007**, *22* (6), 815–822. https://doi.org/10.1016/j.envsoft.2006.03.004.

(40) Gnanapragasam, N.; Reddy, B.; Rosen, M. Reducing CO2 Emissions for an IGCC Power Generation System : Effect of Variations in Gasifier and System Operating Conditions. *Energy Convers. Manag.* **2009**, *50* (8), 1915–1923. https://doi.org/10.1016/j.enconman.2009.04.017.

(41) Charry-Sanchez, J.; Betancourt-Torcat, A.; Ricardez-Sandoval, L. An Optimization Energy Model for the Upgrading Processes of Canadian Unconventional Oil. *Energy* **2014**, *68*, 629–643. https://doi.org/10.1016/j.energy.2014.03.016.

(42) McKendry, P. Energy Production from Biomass (Part 3): Gasification Technologies. *Bioresour. Technol.* **2002**, *83* (1), 55–63. https://doi.org/10.1016/s0960-8524(01)00120-1.

(43) Kunze, C.; Spliethoff, H. Modelling of an IGCC Plant with Carbon Capture for 2020. *Fuel Process. Technol.* **2010**, *91* (8), 934–941. https://doi.org/10.1016/j.fuproc.2010.02.017.

(44) Yeon, D.; Fukasawa, R.; Ricardez-sandoval, L. Bi-Objective Short-Term Scheduling in a Rolling Horizon Framework : A Priori Approaches with Alternative Operational Objectives. *Comput. Oper. Res.* **2019**. https://doi.org/10.1016/j.cor.2019.06.006.

## Nomenclature

| | |
|---|---|
| A | Area ($m^2$) |
| $b_i$ | Bias applied to $i$th neuron |
| C | Concentration ($mole/m^3$) |
| $C_P$ | Heat capacity (J/kg/K) |
| $f$ | Transfer function applied to $\xi_i$ |
| $F'$ | Volumetric force ($N/m^3$) |
| $g$ | Gravitational acceleration ($m/s^2$) |
| h | Convection coefficient ($W/m^2/K$) |
| H | Enthalpy (J/kg) |
| k | Thermal conductivity (W/m/K) |
| m | Mass (kg) |
| m′ | Mass flux ($kg/m^2/s$) |
| M | Mass flow (kg/s) |
| N | Density of particle ($1/m^{-3}$) |
| **P** | Vector of key input parameters |
| $\mathbf{P}_{max}$ | Upper bounds on key input parameters |
| $\mathbf{P}_{min}$ | Lower bounds on key input parameters |
| $\mathbf{P}_{nom}$ | Gasifier nominal operating conditions |
| $P_1$ | Injected fuel flowrate (kg/h) |
| $P_2$ | Oxygen flowrate (kg/h) |
| $P_3$ | Nitrogen flowrate (kg/h) |
| $P_4$ | Steam flowrate (kg/h) |
| $P_5$ | Initial fuel temperature (K) |
| $P_6$ | Mass fraction of ash in fuel |
| $P_7$ | Mass fraction of volatiles in fuel |
| $P_8$ | Mass fraction of moisture in fuel |
| Q′ | Heat flux ($W/m^2$) |

| | |
|---|---|
| $Q'$ | Heat flux (W/m$^2$) |
| r | Radius (m) |
| t | Time (s) |
| $T$ | Temperature (K) |
| **T** | Vector of key output parameters |
| $T_1$ | Carbon conversion |
| $T_{1,max}$ | Maximum gasifier carbon conversion |
| $T_{1,min}$ | Minimum gasifier carbon conversion |
| $T_2$ | Molar composition of CO in the syngas |
| $T_3$ | Molar composition of $H_2$ in the syngas |
| $T_{3,max}$ | Maximum gasifier $H_2$ molar fraction |
| $T_{3,min}$ | Minimum gasifier $H_2$ molar fraction |
| $T_4$ | Peak gasifier temperature (K) |
| $T_{4,max}$ | Maximum allowable peak gasifier temperature (K) |
| $T_5$ | Temperature, thermocouple 1 (K) |
| $T_6$ | Temperature, thermocouple 2 (K) |
| $T_7$ | Temperature, thermocouple 3 (K) |
| $T_8$ | Temperature, thermocouple 4 (K) |
| $u$ | Velocity (m/s) |
| $w$ | Multi-objective significance weight |
| $w_{i,j}$ | Weight applied to $i$th neuron, $j$th input |
| $x$ | Molar fraction |
| $x_j$ | Input value, $j$th input |
| z | Axial domain (m) |
| $\varepsilon$ | Volume fraction |
| $\delta$ | Slag thickness (m) |
| $\xi_i$ | Linear weights function, $i$th neuron |
| $\rho$ | Density (kg/m$^3$) |

## Figure Captions

Table 1
Mathematical model of the multi-phase flow in the ROM

| | |
|---|---|
| **Gas phase** | |
| Momentum | $-\frac{\partial(\mathrm{A}_{cs}\varepsilon_{\mathrm{g}}\rho_{\mathrm{g}}u_{\mathrm{g}}^2)}{\partial \mathrm{x}}+\mathrm{A}_{cs}(-\frac{dP}{dz}+\varepsilon_{\mathrm{g}}\rho_{\mathrm{g}}\mathrm{g}-F'_{\mathrm{g},w}-F'_{\mathrm{g},p})=0$ |
| Mass | $\frac{\partial}{\partial \mathrm{x}}\left(\mathrm{A}_{cs}D_{\mathrm{g,eff}}\frac{\partial(\varepsilon_{\mathrm{g}}\mathrm{C}_{\mathrm{g}_i})}{\partial x}\right)-\frac{\partial\left(\mathrm{A}_{cs}\varepsilon_{\mathrm{g}}u_{\mathrm{g}}\mathrm{C}_{\mathrm{g}_i}\right)}{\partial \mathrm{x}}+\mathrm{A}_{cs}\left(\mathrm{MS}_{\mathrm{g}_i}^{\mathrm{Hetero}}+\mathrm{MS}_{\mathrm{g}_i}^{\mathrm{Homo}}\right)=0$ |
| Energy | $\left(\mathrm{A}_{cs}k_{\mathrm{g,eff}}\frac{\partial T_g}{\partial \mathrm{x}}\right)-\frac{\partial\left(\mathrm{A}_{cs}\varepsilon_{\mathrm{g}}u_{\mathrm{g}}\mathrm{C}_{\mathrm{g}_{\mathrm{total}}}c_{\mathrm{p}_{\mathrm{g}}}T_{\mathrm{g}}\right)}{\partial \mathrm{x}}+\mathrm{A}_{cs}\left(\varepsilon_{\mathrm{g}}\mathrm{HS}^{\mathrm{Hetero}}+\mathrm{HS}_{\mathrm{g}}^{\mathrm{Homo}}\right)+\mathrm{Q}'_{\mathrm{conv\ g\to p}}-\mathrm{Q}'_{\mathrm{conv\ g\to w}}-\mathrm{Q}'_{\mathrm{w\to s}}=0$ |
| **Solid phase** | |
| Momentum | $-\frac{\partial}{\partial \mathrm{x}}\left(\mathrm{A}_{cs}\varepsilon_p\rho_p u_p^2\right)+\mathrm{A}_{cs}\left(\varepsilon_p\rho_p\mathrm{g}+F'_{\mathrm{g},p}\right)=0$ |
| Mass | $-\frac{\partial\left(\mathrm{A}_{cs}\varepsilon_p u_p C_p\right)}{\partial \mathrm{x}}+\mathrm{A}_{cs}\left(\mathrm{MS}_{\mathrm{p}}^{\mathrm{Homo}}\right)-\mathrm{m}'_{\mathrm{slagging}}=0$ |
| Energy | $-\frac{\partial}{\partial \mathrm{x}}\left(\mathrm{A}_{cs}\varepsilon_p u_p C_p c_{p_p}T_p\right)+\mathrm{A}_{cs}\left(\varepsilon_{\mathrm{p}}\mathrm{HS}^{\mathrm{Hetero}}\right)-\mathrm{Q}'_{\mathrm{conv\ p\to g}}-\mathrm{Q}'_{\mathrm{rad\ p\to w}}-\mathrm{m}'_{\mathrm{slagging}}\mathrm{h}_{\mathrm{p}}=0$ |
| Number of particles | $\frac{\partial(\mathrm{A}_{cs}\mathrm{N}_{\mathrm{p}}u_p)}{\partial \mathrm{x}}+\frac{\mathrm{m}'_{\mathrm{slagging}}}{\mathrm{m}_{\mathrm{p}}}=0$ |

Table 2
List of the key gasifier input and output parameters, their nominal values, and the upper and lower input parameter bounds over which the ANNs were trained.

| Input parameters (**P**) | Nominal conditions ($\mathbf{P}_{nom}$) | Lower bound ($\mathbf{P}_{min}$) | Upper bound ($\mathbf{P}_{max}$) |
|---|---|---|---|
| $P_1$: Fuel flowrate (kg/h) | 41.2 | 41.2 | 52.3 |
| $P_2$: $O_2$ flowrate (kg/h) | 37.2 | 28.4 | 37.2 |
| $P_3$: $N_2$ flowrate (kg/h) | 12.1 | 11.0 | 12.1 |
| $P_4$: Steam flowrate (kg/h) | 10.7 | 0 | 21.8 |
| $P_5$: Fuel temperature (K) | 300 | 270 | 330 |
| $P_6$: Mass fraction of ash in fuel | 0.046 | 0.0414 | 0.0506 |
| $P_7$: Mass fraction of volatiles in fuel | 0.127 | 0.1143 | 0.1397 |
| $P_8$: Mass fraction of moisture in fuel | 0.005 | 0.0045 | 0.0055 |
| Output parameters (**T**) | Output values at nominal condition | | |
| $T_1$: Conversion | 0.9134 | | |
| $T_2$: Outlet CO composition | 0.5135 | | |
| $T_3$: Outlet $H_2$ composition | 0.2176 | | |
| $T_4$: Peak temperature (K) | $2.6631 \times 10^3$ | | |
| $T_5$: Temperature: Thermocouple 1 (K) | $1.9114 \times 10^3$ | | |
| $T_6$: Temperature: Thermocouple 2 (K) | $1.7864 \times 10^3$ | | |
| $T_7$: Temperature: Thermocouple 3 (K) | $1.6726 \times 10^3$ | | |
| $T_8$: Temperature: Thermocouple 4 (K) | $1.6090 \times 10^3$ | | |

Table 3
Comparison of the backpropagation algorithms

| BP algorithm | R values | Mean squared error | Iteration number |
|---|---|---|---|
| Levenberg-Marquardt | 0.999 | $2.30\times10^{-7}$ | 138 |
| Scaled conjugate gradient | 0.999 | $6.36\times10^{-7}$ | 363 |
| One-step secant BP | 0.999 | $3.71\times10^{-7}$ | 349 |
| BFGS Quasi-Newton | 0.996 | $1.12\times10^{-5}$ | 128 |
| Gradient descent with momentum and adaptive LR | 0.998 | $1.85\times10^{-4}$ | 227 |
| Gradient descent with momentum | 0.980 | 0.0178 | 1,000 |
| Resilient backpropagation | 0.999 | $1.70\times10^{-6}$ | 600 |
| Gradient descent | 0.998 | 0.0155 | 1,000 |

Table 4

The optimal number of hidden layer neurons, and resulting testing and validation errors, for each output parameter captured by the ANN

| Output parameters | Neuron number | MSE | | Maximum percentage error | |
|---|---|---|---|---|---|
| | | test | validation | test | validation |
| Conversion ($T_1$) | 5 | $4.7259 \times 10^{-6}$ | $4.7259 \times 10^{-6}$ | 2.5641% | 2.6741% |
| CO composition ($T_2$) | 4 | $5.1430 \times 10^{-7}$ | $4.4308 \times 10^{-7}$ | 1.2188% | 1.5834% |
| H2 composition ($T_3$) | 3 | $3.0349 \times 10^{-7}$ | $4.3752 \times 10^{-7}$ | 2.2514% | 1.7657% |
| Peak temperature ($T_4$) | 5 | 47.6507 | 57.6080 | 2.4972% | 2.2134% |
| Thermocouple 1 ($T_5$) | 6 | 46.1238 | 43.5570 | 6.0075% | 5.2366% |
| Thermocouple 2 ($T_6$) | 6 | 15.2896 | 17.2068 | 2.9233% | 2.5796% |
| Thermocouple 3 ($T_7$) | 6 | 3.9126 | 3.6703 | 1.5751% | 1.4401% |
| Thermocouple 4 ($T_8$) | 6 | 2.2825 | 2.6484 | 0.7688% | 1.2136% |

Table 5
First ten combination of input parameters used to validate the ANN

| Input parameter | 1 | 2 | 3 | 4 | 5 | 6 | 7 | 8 | 9 | 10 |
|---|---|---|---|---|---|---|---|---|---|---|
| $P_1$ (Fuel flowrate, kg/h) | 44.93 | 48.19 | 50.80 | 43.67 | 45.42 | 43.60 | 46.11 | 46.68 | 49.68 | 42.90 |
| $P_2$ ($O_2$ flowrate, kg/h) | 35.48 | 34.31 | 32.08 | 31.57 | 29.40 | 29.18 | 30.06 | 36.48 | 35.22 | 35.87 |
| $P_3$ ($N_2$ flowrate, kg/h) | 11.40 | 11.63 | 11.37 | 11.28 | 11.62 | 11.89 | 12.02 | 11.91 | 11.99 | 11.63 |
| $P_4$ (Steam flowrate, kg/h) | 20.46 | 0.12 | 20.99 | 18.05 | 16.46 | 16.39 | 3.92 | 6.72 | 20.42 | 6.01 |
| $P_5$ (Fuel temperature, K) | 280.24 | 277.59 | 324.90 | 313.38 | 309.90 | 319.86 | 306.71 | 287.15 | 272.94 | 321.78 |
| $P_6$ (Mass fraction of ash) | 0.0466 | 0.0484 | 0.0469 | 0.0452 | 0.0498 | 0.0429 | 0.0428 | 0.0470 | 0.0490 | 0.0449 |
| $P_7$ (Mass fraction of volatiles) | 0.1389 | 0.1346 | 0.1392 | 0.1376 | 0.1277 | 0.1390 | 0.1210 | 0.1272 | 0.1267 | 0.1269 |
| $P_8$ (Mass fraction of moisture) | 0.0046 | 0.0048 | 0.0048 | 0.0051 | 0.0047 | 0.0050 | 0.0054 | 0.0047 | 0.0049 | 0.0050 |

Table 6

The mean squared, mean, and maximum errors obtained for all eight output parameters over 2,500 input combinations

| Output parameters | MSE | Mean error | Max error |
|---|---|---|---|
| $T_1$ (Conversion) | $4.7259 \times 10^{-6}$ | 0.2204% | 2.5641% |
| $T_2$ (CO composition) | $3.1658 \times 10^{-7}$ | 0.0662% | 1.4744% |
| $T_3$ ($H_2$ composition) | $4.2342 \times 10^{-7}$ | 0.2085% | 1.5247% |
| $T_4$ (Peak temperature, K) | 60.8380 | 0.1740% | 2.1374% |
| $T_5$ (Thermocouple 1, K) | 45.5503 | 0.1421% | 5.3596% |
| $T_6$ (Thermocouple 2, K) | 17.4942 | 0.1236% | 2.8246% |
| $T_7$ (Thermocouple 3, K) | 3.5040 | 0.0532% | 1.7441% |
| $T_8$ (Thermocouple 4, K) | 2.5240 | 0.0523% | 1.0516% |

Table 7 Carbon conversion optimization results

| parameter name | Nominal condition | Case 1 ($T_{4,max}$ =2400K) | Case 2 ($T_{4,max}$ =2500K) | Case 3 ($T_{4,max}$ =2600K) | Case 4 ($T_{4,max}$ = 2700K) |
|---|---|---|---|---|---|
| $P_1$ (Fuel Flow Rate, kg/h) | 41.2 | 40 | 40 | 40 | 40 |
| $P_2$ ($O_2$ Flow Rate, kg/h) | 37.2 | 30.8921 | 34.449 | 37.2 | 37.2 |
| $P_3$ ($N_2$ Flow Rate, kg/h) | 12.1 | 12.1 | 12.1 | 11 | 11 |
| $P_4$ (Steam Flow Rate, kg/h) | 10.7 | 21.8 | 21.8 | 19.2112 | 19.2111 |
| $P_5$ (Fuel Temperature, K) | 300 | 330 | 330 | 330 | 330 |
| $P_6$ (Mass Fraction Ash) | 0.046 | 0.0506 | 0.0506 | 0.0506 | 0.0506 |
| $P_7$ (Mass Fraction Volatiles) | 0.127 | 0.1397 | 0.1397 | 0.1397 | 0.1397 |
| $P_8$ (Mass Fraction Moisture) | 0.005 | 0.0055 | 0.0055 | 0.0055 | 0.0055 |
| Optimized parameter | | | | | |
| $T_1$ (Conversion) in optimization using ANN | | 0.8111 | 0.9033 | 0.9702 | 0.9702 |
| $T_1$ (Conversion) run by ROM | 0.9134 | 0.8114 | 0.9009 | 0.9690 | 0.9690 |
| Relative error | | 0.04% | 0.27% | 0.12% | 0.12% |
| Parameter in constrain | | | | | |
| $T_4$ (Peak temperature, K) in optimization using ANN | | 2400 | 2500 | 2600 | 2620.2 |
| $T_4$ (Peak temperature, K) run by ROM | 2663.1 | 2399.8 | 2501 | 2605.3 | 2627.2 |
| Relative error | | 0.01% | 0.04% | 0.20% | 0.27% |
| $T_2$ (CO molar fraction) results using ANN | | 0.3616 | 0.3897 | 0.4345 | 0.4345 |
| $T_3$ ($H_2$ molar fraction) results using ANN | | 0.2542 | 0.245 | 0.24 | 0.24 |
| $T_5$ (Thermocouple 1 Temperature, K) results using ANN | | 1778.80 | 1845.50 | 1896.40 | 1896.40 |
| $T_6$ (Thermocouple 2 Temperature, K) results using ANN | | 1664.90 | 1733.20 | 1779.10 | 1779.10 |
| $T_7$ (Thermocouple 3 Temperature, K) results using ANN | | 1564.30 | 1620.00 | 1663.00 | 1663.00 |
| $T_8$ (Thermocouple 4 Temperature, K) results using ANN | | 1502.40 | 1555.50 | 1598.30 | 1598.30 |

| parameter name | w = 0 | w = 0.1 | w = 0.2 | w = 0.3 | w = 0.4 | w = 0.5 | w = 0.6 | w = 0.7 | w = 0.8 | w = 0.9 | w = 1 | 1-norm |
|---|---|---|---|---|---|---|---|---|---|---|---|---|
| $P_1$ (Fuel Flow Rate, kg/h) | 40 | 40 | 40 | 40 | 40 | 40 | 40 | 40 | 40 | 40 | 52.3 | 40 |
| $P_2$ ($O_2$ Flow Rate, kg/h) | 37.2 | 37.2 | 37.2 | 37.2 | 37.2 | 37.2 | 37.2 | 37.2 | 37.2 | 28.4 | 28.4 | 28.4 |
| $P_3$ ($N_2$ Flow Rate, kg/h) | 11 | 11 | 11 | 11 | 11 | 11 | 11 | 11 | 11 | 11 | 11 | 11 |
| $P_4$ (Steam Flow Rate, kg/h) | 19.2112 | 19.5424 | 19.9225 | 20.366 | 20.8952 | 21.5464 | 21.8 | 21.8 | 21.8 | 18.1061 | 14.5294 | 18.0935 |
| $P_5$ (Fuel Temperature, K) | 330 | 330 | 330 | 330 | 330 | 330 | 330 | 330 | 330 | 330 | 330 | 330 |
| $P_6$ (Mass Fraction Ash) | 0.0506 | 0.0506 | 0.0506 | 0.0506 | 0.0506 | 0.0506 | 0.0506 | 0.0506 | 0.0506 | 0.0506 | 0.0506 | 0.0506 |
| $P_7$ (Mass Fraction Volatiles) | 0.1397 | 0.1397 | 0.1397 | 0.1397 | 0.1397 | 0.1397 | 0.1397 | 0.1397 | 0.1397 | 0.1397 | 0.1397 | 0.1397 |
| $P_8$ (Mass Fraction Moisture) | 0.0055 | 0.0055 | 0.0055 | 0.0055 | 0.0055 | 0.0045 | 0.0055 | 0.0055 | 0.0055 | 0.0045 | 0.0045 | 0.0045 |
| Optimized parameter | | | | | | | | | | | | |
| $T_1$ (Conversion) results using ANN | 0.9702 | 0.9702 | 0.9701 | 0.9701 | 0.9699 | 0.9697 | 0.9696 | 0.9696 | 0.9696 | 0.7494 | 0.5471 | 0.7494 |
| $T_1$ (Conversion) results using ROM | 0.9690 | 0.9690 | 0.9689 | 0.9688 | 0.9687 | 0.9684 | 0.9683 | 0.9683 | 0.9683 | 0.7492 | 0.5476 | 0.7492 |
| Relative error | 0.12% | 0.12% | 0.12% | 0.13% | 0.12% | 0.13% | 0.13% | 0.13% | 0.13% | 0.03% | 0.09% | 0.03% |
| | | | | | | | | | | | | |
| $T_3$ ($H_2$ molar fraction) results using ANN | 0.2400 | 0.2401 | 0.2404 | 0.2406 | 0.2408 | 0.2411 | 0.2412 | 0.2412 | 0.2412 | 0.265 | 0.2836 | 0.265 |
| $T_3$ ($H_2$ molar fraction) results using ROM | 0.2354 | 0.2356 | 0.2357 | 0.2358 | 0.2359 | 0.2360 | 0.2360 | 0.2360 | 0.2360 | 0.2638 | 0.2843 | 0.2638 |
| Relative error | 1.95% | 1.91% | 1.99% | 2.04% | 2.08% | 2.16% | 2.20% | 2.20% | 2.20% | 0.45% | 0.25% | 0.45% |
| | | | | | | | | | | | | |
| $T_2$ (CO molar fraction) results using ANN | 0.4345 | 0.4317 | 0.4285 | 0.4247 | 0.4203 | 0.4157 | 0.413 | 0.413 | 0.413 | 0.3755 | 0.3704 | 0.3756 |
| $T_4$ (Peak temperature, K) in optimization using ANN | 2596.60 | 2594.50 | 2592.20 | 2589.50 | 2586.30 | 2583.50 | 2581.20 | 2581.20 | 2581.20 | 2346.00 | 2245.30 | 2346.10 |
| $T_5$ (Thermocouple 1 Temperature, K) results using ANN | 1896.40 | 1896.10 | 1895.80 | 1895.50 | 1895.10 | 1894.00 | 1894.70 | 1894.70 | 1894.70 | 1735.90 | 1679.60 | 1735.90 |
| $T_6$ (Thermocouple 2 Temperature, K) results using ANN | 1779.10 | 1779.10 | 1779.20 | 1779.30 | 1779.50 | 1780.20 | 1780.00 | 1780.00 | 1780.00 | 1617.90 | 1561.10 | 1617.90 |
| $T_7$ (Thermocouple 3 Temperature, K) results using ANN | 1663.00 | 1662.80 | 1662.60 | 1662.40 | 1662.20 | 1661.50 | 1662.00 | 1662.00 | 1662.00 | 1520.40 | 1469.10 | 1520.40 |
| $T_8$ (Thermocouple 4 Temperature, K) results using ANN | 1598.30 | 1598.20 | 1598.10 | 1598.00 | 1598.00 | 1597.90 | 1598.00 | 1598.00 | 1598.00 | 1462.20 | 1411.40 | 1462.20 |

Table 8 Multi-objective optimization results

Figure 1

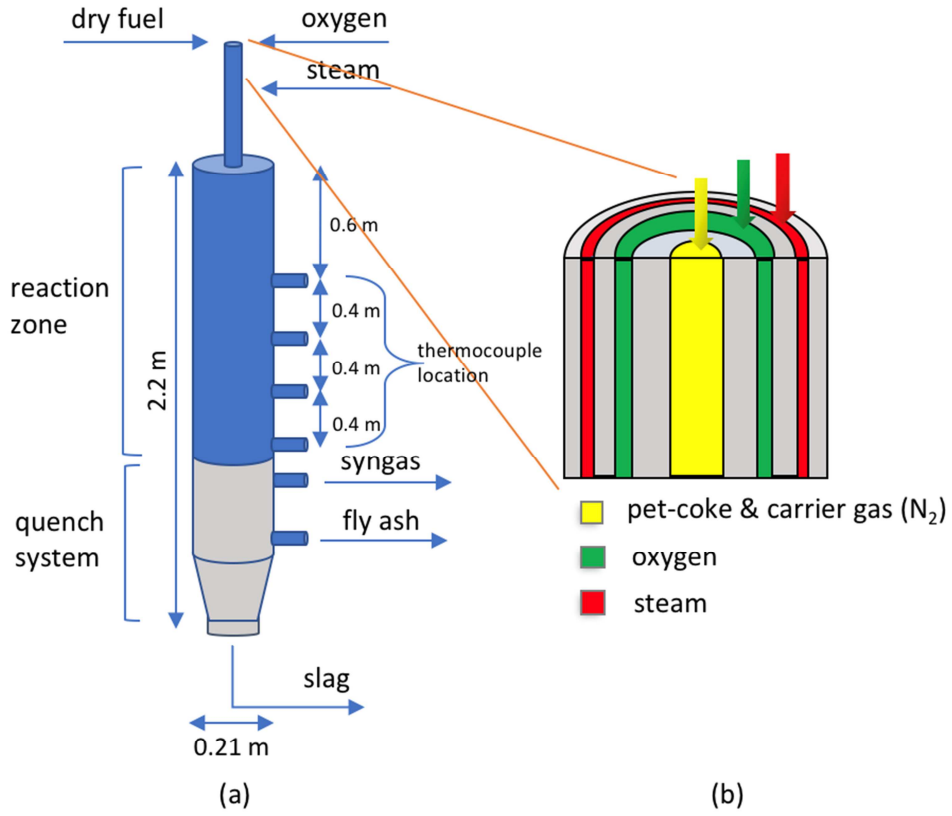
dry fuel
oxygen
steam
0.6 m
reaction zone
0.4 m
0.4 m
0.4 m
thermocouple location
2.2 m
syngas
quench system
fly ash
slag
0.21 m
(a)
pet-coke & carrier gas ($N_2$)
oxygen
steam
(b)

Figure 2

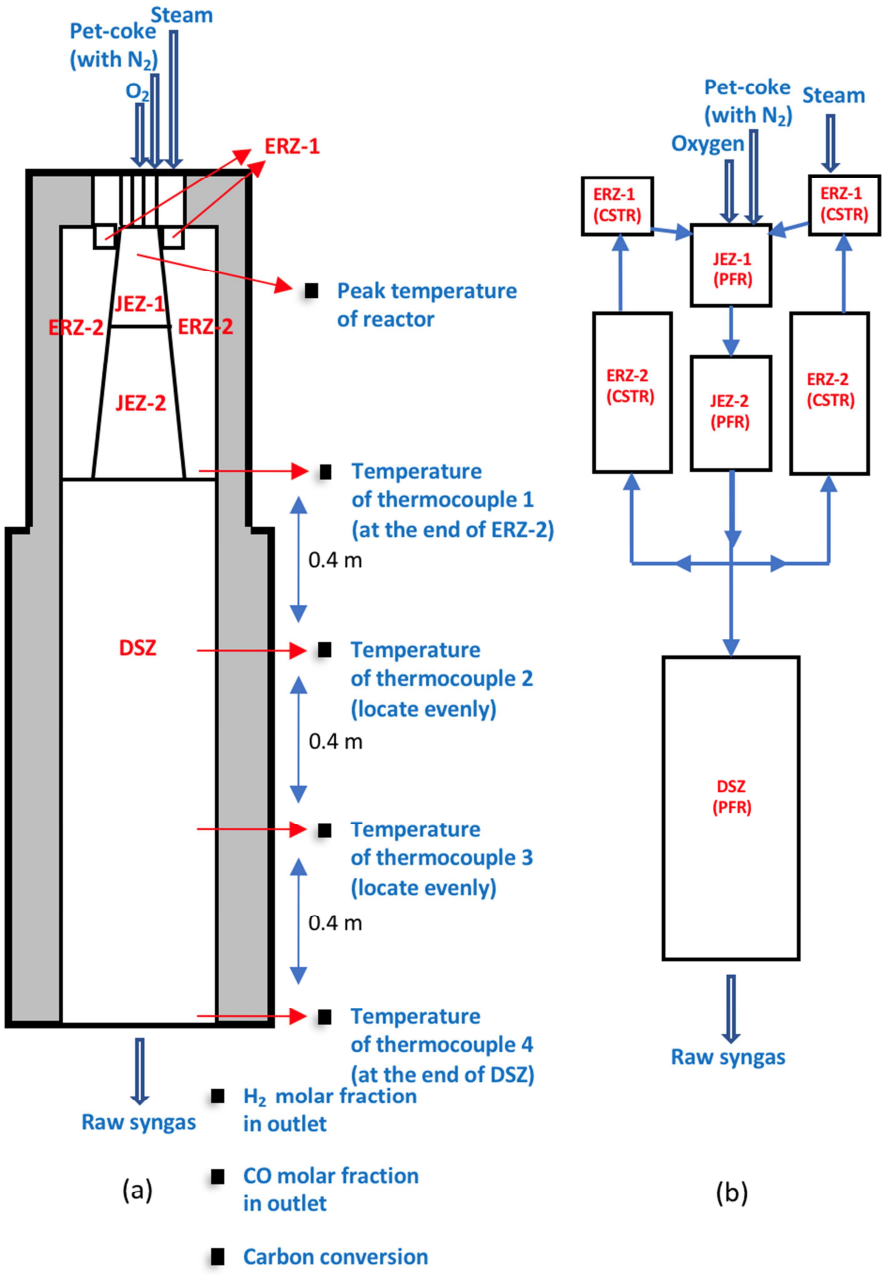
Pet-coke (with $N_2$)
Steam
$O_2$
ERZ-1
JEZ-1
ERZ-2
ERZ-2
JEZ-2
Peak temperature of reactor
Temperature of thermocouple 1 (at the end of ERZ-2)
0.4 m
DSZ
Temperature of thermocouple 2 (locate evenly)
0.4 m
Temperature of thermocouple 3 (locate evenly)
0.4 m
Temperature of thermocouple 4 (at the end of DSZ)
Raw syngas
$H_2$ molar fraction in outlet
CO molar fraction in outlet
Carbon conversion
(a)
Pet-coke (with $N_2$)
Oxygen
Steam
ERZ-1 (CSTR)
ERZ-1 (CSTR)
JEZ-1 (PFR)
ERZ-2 (CSTR)
JEZ-2 (PFR)
ERZ-2 (CSTR)
DSZ (PFR)
Raw syngas
(b)

Figure 3

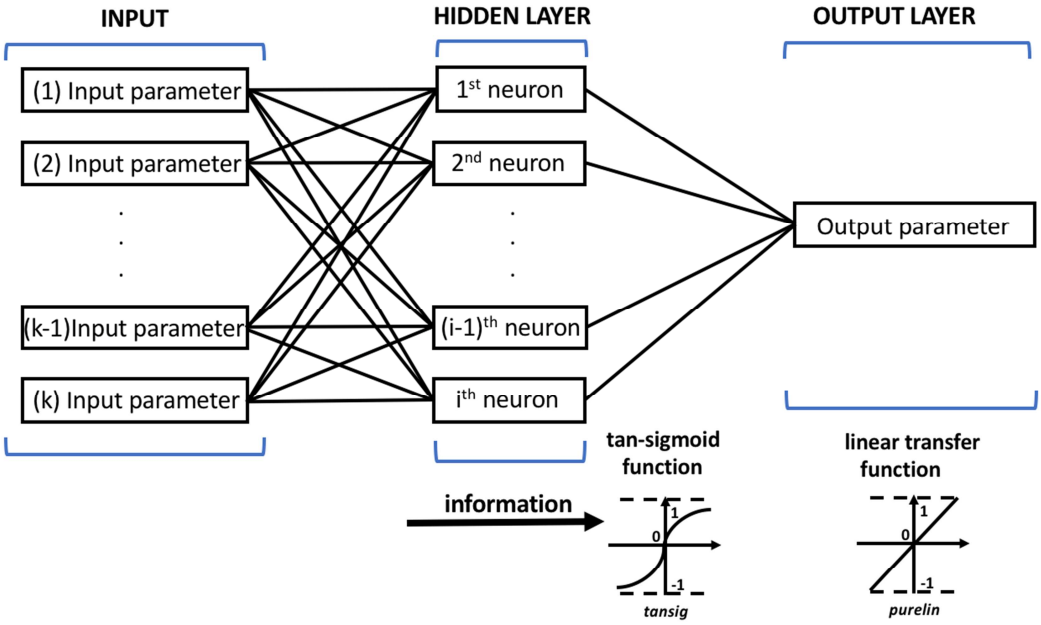

Figure 4

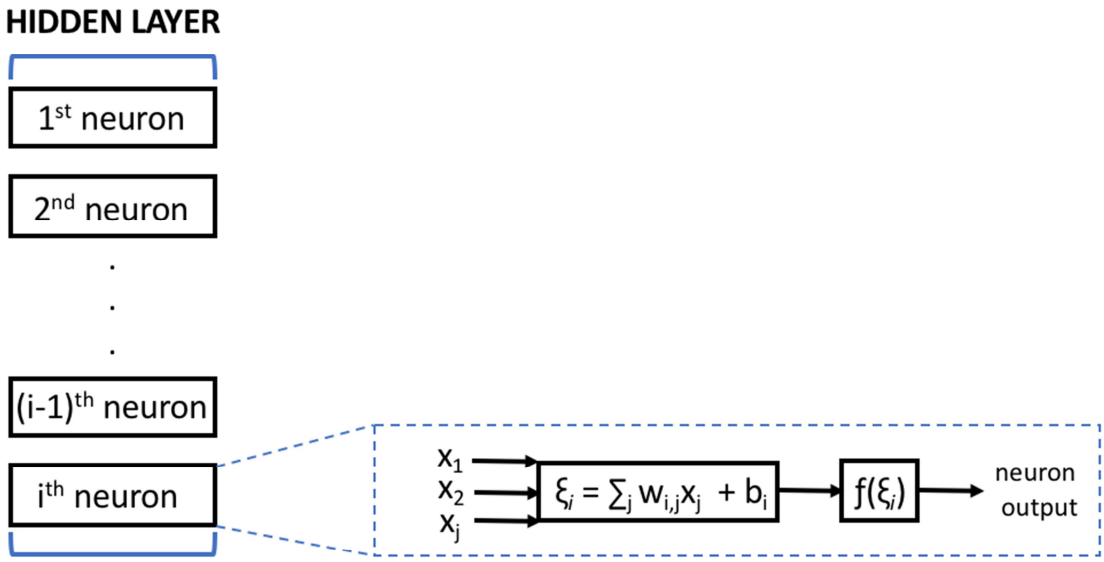

Figure 5

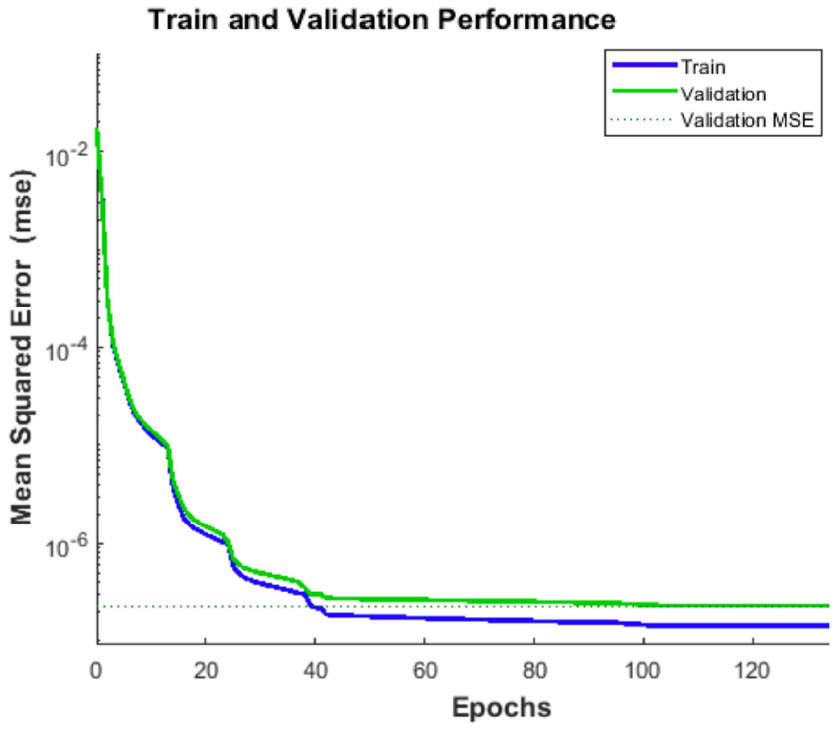

Figure 6

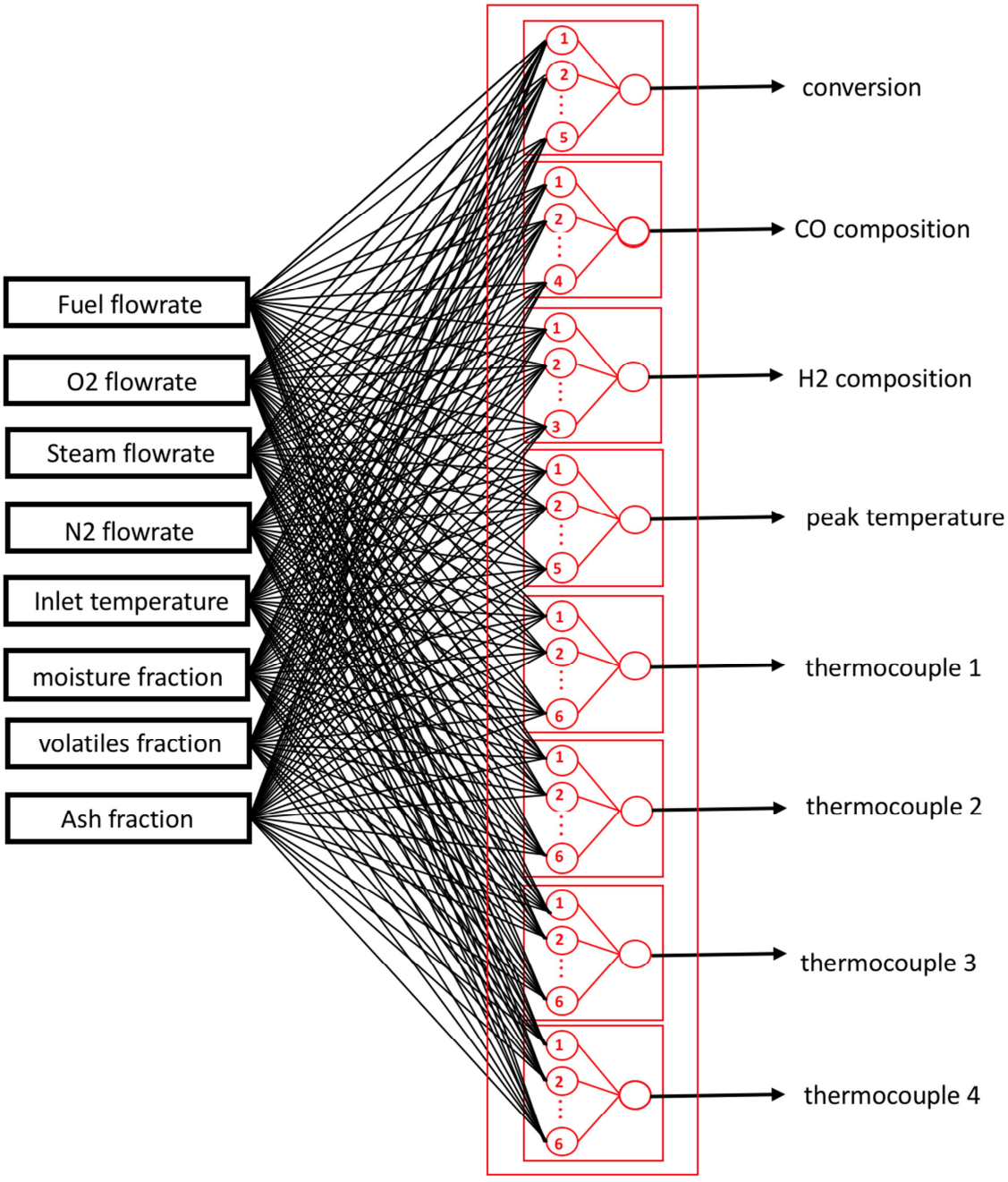
Fuel flowrate
O2 flowrate
Steam flowrate
N2 flowrate
Inlet temperature
moisture fraction
volatiles fraction
Ash fraction
conversion
CO composition
H2 composition
peak temperature
thermocouple 1
thermocouple 2
thermocouple 3
thermocouple 4

Figure 7

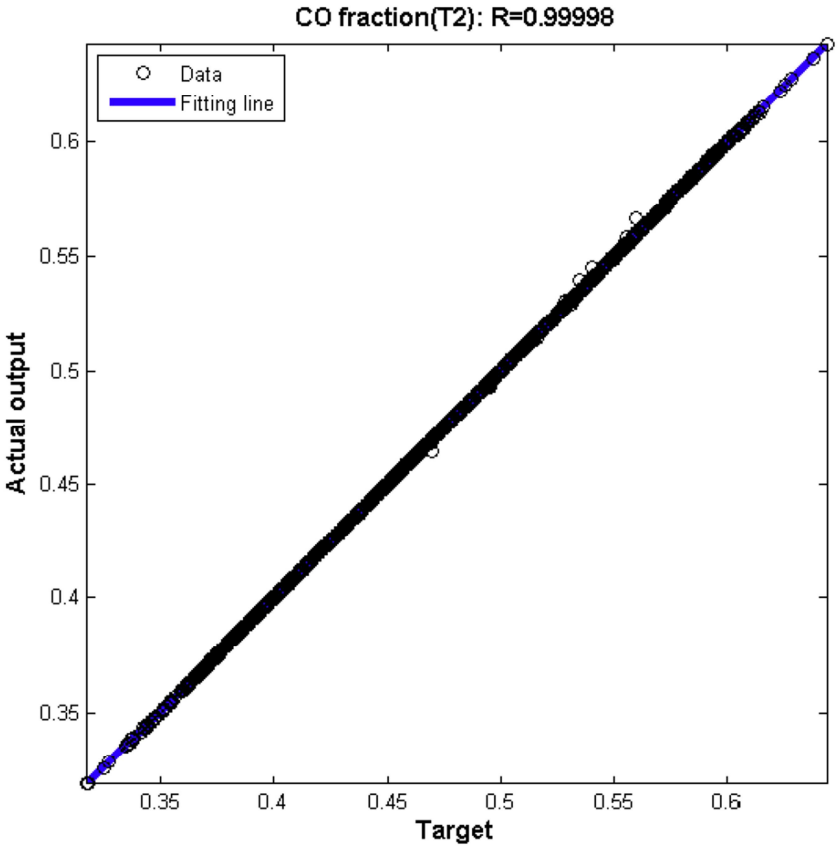
CO fraction(T2): R=0.99998
Data
Fitting line
Actual output
Target
0.6
0.55
0.5
0.45
0.4
0.35
0.35
0.4
0.45
0.5
0.55
0.6

Figure 8

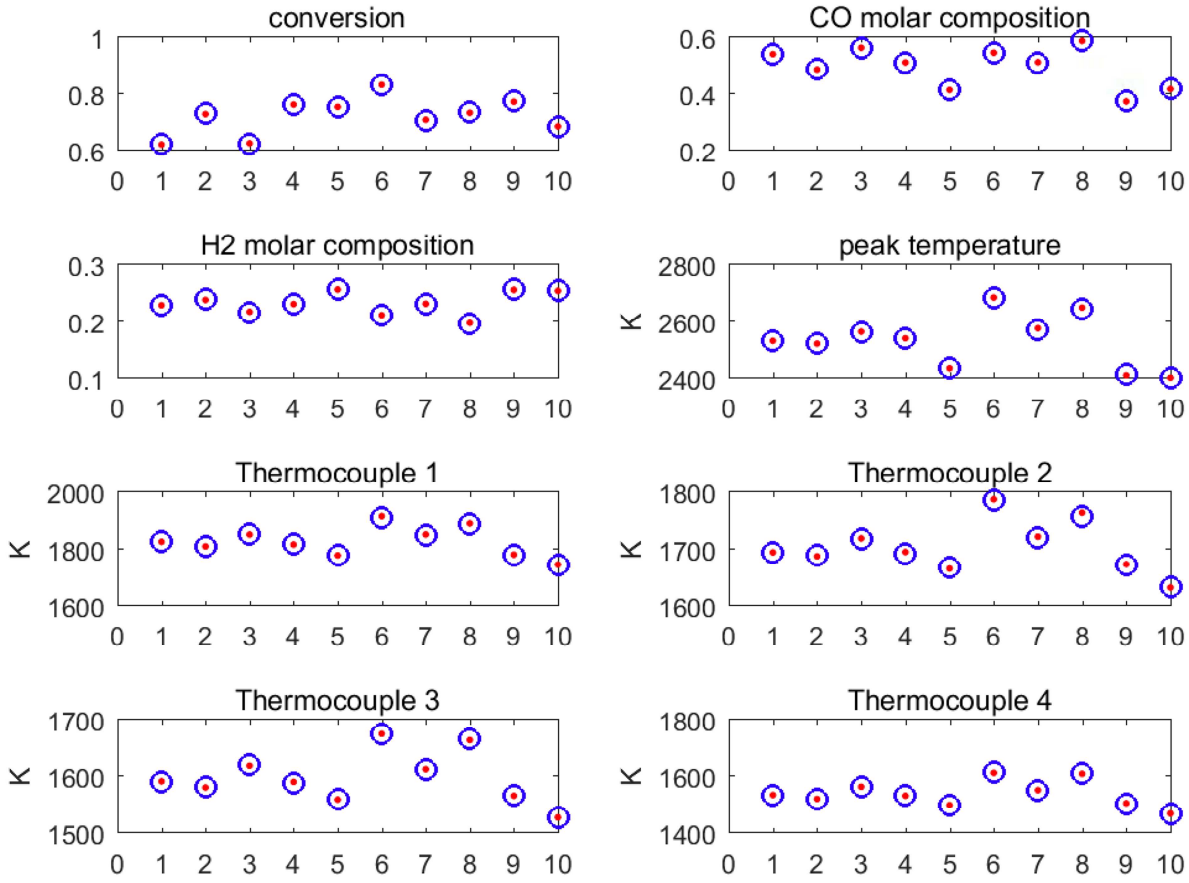
conversion
CO molar composition
H2 molar composition
peak temperature
Thermocouple 1
Thermocouple 2
Thermocouple 3
Thermocouple 4
K

Figure 9

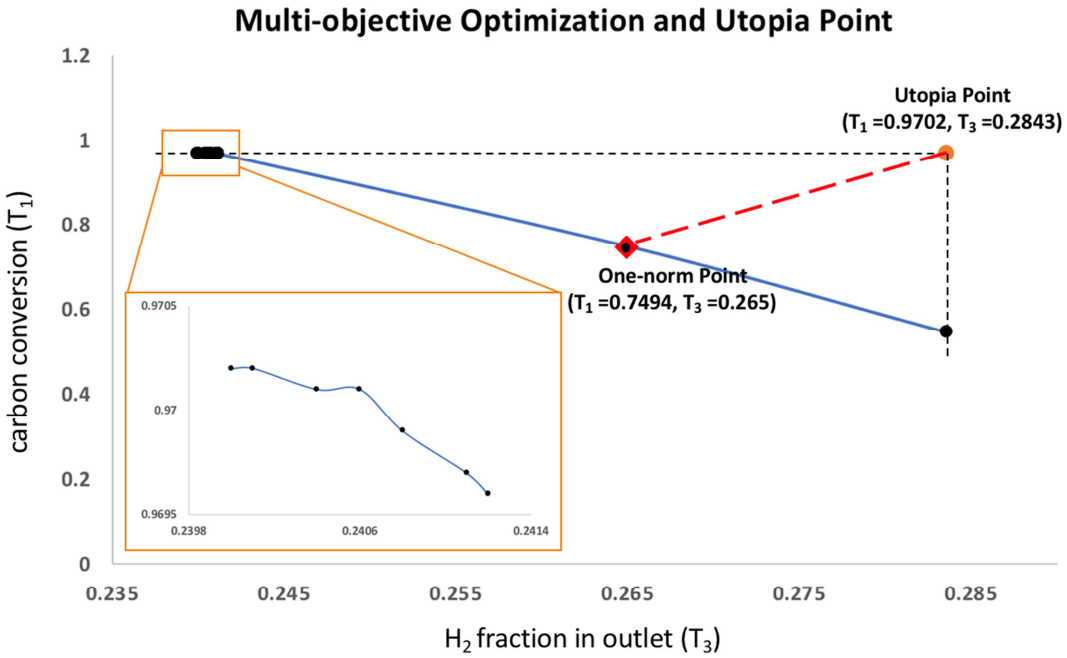

Highlights

- The design of an artificial nueral networks model on a pilot-scale gasifier is presented
- Optimization studies using the ANN gasification model were performed and validated
- ANN model is at least 4 orders of magnitude faster than reduced order models

**Declaration of interests**

☒ The authors declare that they have no known competing financial interests or personal relationships that could have appeared to influence the work reported in this paper.

☐The authors declare the following financial interests/personal relationships which may be considered as potential competing interests:

Sincerely,

Luis Ricardez-Sandoval
Associate Professor, University of Waterloo
Corresponding author signing on behalf of all the authors of this work
Email: laricard@uwaterloo.ca